Scanning Mobility CCN Analysis: A method for fast measurements of size-resolved CCN distributions and activation kinetics

Richard H. Moore

School of Chemical & Biomolecular Engineering, Georgia Institute of Technology

Athanasios Nenes

Schools of Earth & Atmospheric Sciences and Chemical & Biomolecular Engineering, Georgia Institute of Technology

Jeessy Medina

School of Chemical & Biomolecular Engineering, Georgia Institute of Technology

Abstract. We present Scanning Mobility CCN Analysis (SMCA) as a novel method for obtaining rapid measurements of size-resolved cloud condensation nuclei (CCN) distributions and activation kinetics. SMCA involves sampling the monodisperse outlet stream of a Differential Mobility Analyzer (DMA) operated in scanning voltage mode concurrently with CCN and condensation particle counters. By applying the same inversion algorithm as used for obtaining size distributions with a scanning mobility particle sizer (SMPS), CCN concentration and activated droplet size are obtained as a function of mobility size over the timescale of an SMPS scan (typically 60-120s). Methods to account for multiple charging, non-sphericity effects and limited counting statistics are presented. SMCA is demonstrated using commercial SMPS and CFSTGC instruments with the manufacturer-provided control software. The method is evaluated for activation of both laboratory aerosol and ambient aerosol obtained during the NEAQS-ITCT2k4 field campaign. It is shown that SMCA reproduces the results obtained with a DMA operating in voltage "stepping" mode.

1. Introduction

Predictive understanding of aerosol-cloud interactions in climate and hydrological cycle studies (e.g., *Intergovernmental Panel on Climate Change (IPCC)* [2007]; *International Aerosol Precipitation Science Assessment Group (IAPSAG)* [2007]) requires a global network of cloud condensation nuclei (CCN) measurements. With the advent of the Continuous-Flow Streamwise Thermal Gradient CCN Chamber (CFSTGC; *Roberts and Nenes* [2005]) and its commercialization by Droplet Measurement Technologies [*Lance et al.*, 2006; *Rose et al.*, 2008], this is rapidly becoming a reality.

CCN instruments can be utilized in various ways to complement aerosol-cloud interaction studies. They can be used as "counters", where the concentration of CCN is measured at a given level of supersaturation. This mode of operation is commonly used for "CCN closure" studies, i.e., to assess the ability of thermodynamic theory to predict CCN concentrations from measurements of aerosol size distribution and chemical composition [e.g., *Rose et al.*, 2010; *Jurányi et al.*, 2010; *Bougiatioti et al.*, 2009; *Lance et al.*, 2009; *Cubison et al.*, 2008; *Sorooshian et al.*, 2008; *Wang et al.*, 2008; *Vestin et al.*, 2007; *Medina et al.*, 2007; *Broekhuizen et al.*, 2006, and others]. The maximum potential of CCN measurements is realized when CCN instruments, operating in either counting mode or in "spectrometer" mode [*Moore and*

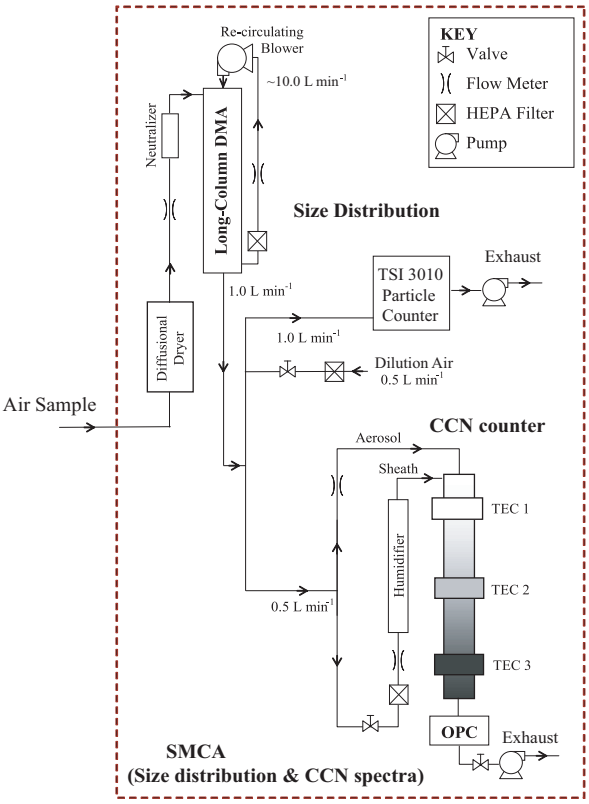

Figure 1. Schematic of the setup used for the Scanning Mobility CCN Analysis (SMCA).

Nenes, 2009], are coupled with a differential mobility analyzer (DMA) to obtain size-resolved measurements. These methods provide the CCN concentration across supersaturations and particle sizes, which when coupled with theory, enables the parameterization of composition impacts on cloud droplet formation [e.g., *Rose et al.*, 2010; *Petters et al.*, 2009; *Dusek et al.*, 2010; *Carrico et al.*, 2008; *Petters and Kreidenweis*, 2007; *Wex et al.*, 2007; *Padró et al.*, 2007, 2010; *Padró*, 2009; *Lance*, 2007], the characterization of chemical ageing and mixing state of aerosol [e.g., *Shinozuka et al.*, 2009; *Cubison et al.*, 2008; *Kuwata et al.*, 2008; *Lance*, 2007; *Padró*, 2009], and the evaluation of CCN activation kinetics [e.g., *Asa-Awuku et al.*, 2009; *Shantz et al.*, 2009; *Sorooshian et al.*, 2008; *Ruehl and Nenes*, 2008; *Ruehl et al.*, 2009]. Under certain conditions, size-resolved measurements allow for the inference of average molar volume and surfactant characteristics of the water-soluble carbonaceous aerosol fraction [e.g., *Padró et al.*, 2007; *Asa-Awuku et al.*, 2008, 2010, 2009; *Engelhart et al.*, 2008; *Moore et al.*, 2008; *Padró et al.*, 2010].

Most studies to date operate the DMA in "stepping mode", where the voltage applied to the DMA is held constant during a CCN measurement; the voltage is increased stepwise for another CCN measurement to cover the entire size range of the DMA [e.g., *Rose et al.*, 2010; *Gunthe et al.*, 2009; *Petters et al.*, 2009; *Asa-Awuku et al.*, 2008; *Petters et al.*, 2007, and others]. The technique described in this manuscript, entitled "Scanning Mobility CCN Analysis" (SMCA), provides an alternative method for performing size-resolved CCN measurements; the DMA is operated as a Scanning Mobility Particle Sizer and the voltage is ramped exponentially, typically over a period of 60-120 seconds [*Wang and Flagan*, 1989]. SMCA has been successfully applied in a number of studies [*Padró et al.*, 2007; *Asa-Awuku et al.*, 2008, 2010, 2009; *Engelhart et al.*, 2008; *Moore et al.*, 2008; *Padró et al.*, 2010] and presented in detail here. SMCA can be applied to commercial SMPS and CFSTGC instruments with the manufacturer-provided control software coupled with a simple post-processing routines (available for download from http://nenes.eas.gatech.edu). In subsequent sections, we present SMCA, an overview of the data analysis, and validation of the method with both laboratory aerosol and ambient aerosol sampled during the 2004 ICARTT-ITCT2k4 field campaign.

2. Description of SMCA

2.1. Instrumentation Setup

The instrumentation setup is shown in Figure 1. Polydisperse dry aerosol is charge-neutralized using a Kr-85 neutralizer (TSI 3077A) and introduced into a differential mobility analyzer (DMA, TSI 3081L) for classification by electrical mobility. The classified aerosol is then split between a condensation particle counter (CPC, TSI 3010 or 3022a) for measurement of total aerosol (condensation nuclei, CN) concentration, and a Droplet Measurement Technologies Continuous-Flow, Streamwise Thermal-Gradient Chamber (CFSTGC) [*Roberts and Nenes*, 2005; *Lance et al.*, 2006; *Rose et al.*, 2008] to measure CCN concentrations. In order to maintain a sample flow rate of 1 LPM through the DMA, filtered make-up air is supplied to the classified aerosol stream or to the CPC stream (the latter being preferable in cases where low aerosol concentrations limit the counting statistics in the CFSTGC). In this study, the voltage applied to the DMA is exponentially scanned using the TSI Aerosol Instrument Manager control software, which also manages data acquisition in the CPC and inversion to provide the aerosol number size distribution. The software also provides the raw CN counts

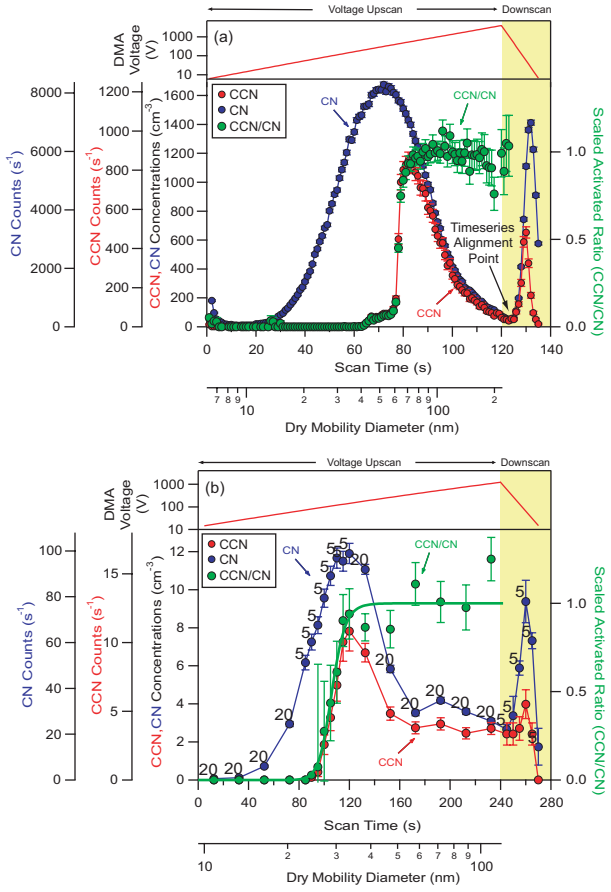

Figure 2. Example of CCN (red), CN (blue) timeseries and inverted activation curve (green). CCN, CN data are presented in terms of raw counts accumulated over 1s, and the corresponding concentrations. Error bars represent the propagated uncertainty, calculated using Equations 5 to 6. Results shown for laboratory-generated aerosol with a total number concentration of (a) 4x10^5 cm^{-3}, and (b) 200 cm^{-3}. Counting statistics limitations are addressed by averaging (post-measurement) consecutive 1s bins, the number of which is noted beside each point.

reported by the CPC every 0.1 s during each scan cycle. While not further discussed here, any instrument control software could be used to control and invert the SMPS data.

The CFSTGC consists of a cylindrical growth chamber with internally-wetted walls upon which a constant streamwise temperature gradient is applied. The difference between the diffusivity of heat and water vapor generates a supersaturation that depends on the flow rate, the streamwise temperature gradient and the pressure in the chamber. Figure 1 illustrates the components and flow diagram of the CFSTGC. The inlet flow is first split into "sheath" and "sample" flows. The latter is directed to the center of the growth chamber, whereas the "sheath" flow is filtered and humidified prior to its entry in the chamber. Both flows travel through the column, exposing aerosol about the centerline to an approximately constant supersaturation (after the decay of entry length effects), a fraction of which activate to form cloud droplets. An optical particle counter (OPC) then counts and sizes the activated droplets at the outlet of the column. The CCN counts are accumulated over a time period of 1s. The relationship between instrument supersaturation and operating conditions (column temperature gradient, flow rate and column pressure) is determined using calibration aerosol, following the procedure of *Lance et al.* [2006], *Rose et al.* [2008], and *Bougiatioti et al.* [2009].

2.2. Application of SMCA

The DMA voltage is continuously cycled between a minimum and maximum value, and the timeseries of CN and CCN counts are recorded (examples are presented in Figure 2a, 2b for high and low aerosol concentration, respectively). The particle size distribution is then obtained from the CN timeseries using well-established SMPS inversion techniques (e.g., *Crump and Seinfeld* [1982]; *Hagen and Alofs* [1983]; *Wang and Flagan* [1989]; *Russell et al.* [1995]; *Collins et al.* [2002]). In this study, the CN timeseries is inverted using the TSI AIM software (which uses the method of *Wang and Flagan* [1989]). The timeseries of CN, CCN is used to determine the "activation" ratio of CCN to CN concentration, R_a, (see right ordinate axis in Figure 2) and applied to the inverted aerosol size distribution to obtain the CCN size distribution (discussed in section 2.3).

For this study, the centroid mobility diameter obtained from the DMA ranged between 10 and 300 nm, size distribution scans were obtained every 135 or 270 seconds (120/240 seconds for the voltage "upscan", and, 15/30 seconds for the voltage "downscan", respectively), where the longer scan time was applied for low concentration measurements to improve counting statistics. The sample flow rate in the DMA was adjusted to be 1 L min^{-1} and the sheath-to-aerosol flow was maintained at a 10:1 or 5:1 ratio. The TSI 3010 CPC (used in the field experiments) operates at 1 L min^{-1}, while the TSI 3022a (used in the laboratory experiments) operates at 1.5 L min^{-1} (with a 0.3 L min^{-1} internal flow). The CCN counter was operated at a flow rate of 0.5 L

min^{-1} at a sheath-to-aerosol flow ratio of 10:1. The supersaturation at the CCN counter is changed every 3-4 voltage scan cycles in the DMA (by changing either the flow rate or the streamwise temperature gradient). Whenever the temperature gradient is changed, up to 2 minutes are required for the instrument profiles to stabilize.

2.3. Data Inversion and Multiple Charge Correction

The inversion to obtain CCN and CN size distributions is applied to the data collected during the voltage upscan. The CPC and CCN counts time series are obtained from the AIM software and CFSTGC software, respectively, and are normalized by flow rate to express them in terms of number concentration. The time series are aligned by matching the minimum in counts that occurs during the transition between upscan and downscan (Figure 2). Owing to the longer plumbing time associated with the CFSTGC, its minimum occurs some fixed time after the corresponding CPC signal (here about 15 seconds). After alignment, the CCN time series is mapped into size space using the size-scantime relationship provided by the AIM software (which uses the voltage-time relationship used in the DMA, accounting for the plumbing time between DMA and CPC and assuming that particles carry a single charge). The aerosol number distribution is then inverted, and R_a determined from the CPC/CCN timeseries is used to obtain the CCN number distribution.

Since the timeseries are influenced by multiple charged particles, it is necessary to rebin the CN and CCN counts based on an equilibrium charge distribution. The following procedure is used:

1. The aerosol number size distribution, $n_n(D_p)$, is obtained by inversion of the CPC timeseries (here using the TSI AIM software).

2. The aligned CN and CCN timeseries are binned to a common time grid. The grid spacing by default is 1s (the reporting time of the CFSTGC), although it can vary to ensure sufficient counting statistics.

3. An estimate of the size-dependent activation efficiency, $R_a^*(D_p) = C_{CCN}(D_p)/C_{CN}(D_p)$, is obtained from the CCN and CN timeseries and the size-scantime relationship provided by the AIM software.

4. The CCN and CN timeseries are then corrected for multiple-charging. Starting from the largest aerosol size bin of the CN timeseries (and moving to each successive smaller bin), the number of particles with +2 and +3 charges are removed and placed in the CN timeseries bin with the correct mobility diameter. The procedure starts from the largest size, because an impactor is placed in front of the sample flow of the DMA, so that the largest size bin in the inverted distributions (corresponding to the 50% cutoff diameter of the impactor) contains only singly-charged particles.

   The number of multiply-charged particles is computed assuming equilibrium charging in the aerosol neutralizer. For particles with n=+1,+2 charges, expressions from *Wiedensohler* [1988] is used to compute the fraction of particles with dry size D_p (here equal to the centroid mobility diameter of each aerosol size bin) and n charges, $f(D_p, n)$,

$$f(D_p, n) = 10^{\left(\sum_{i=0}^{5} a_i(n)(\log D_p)^i\right)} \tag{1}$$

   where $a_i(n)$ are empirical coefficients presented in *Wiedensohler* [1988]. For n =+3, the parameterization presented in *TSI* [2003]; *Gunn* [1955]; *Gunn and Woessner* [1956] is used,

$$f(D_p, +3) = \Phi \exp \frac{-\left(n - \frac{2\pi\varepsilon_0 D_p kT}{e^2} \ln\left(\frac{Z_{i+}}{Z_{i-}}\right)\right)^2}{4\pi\varepsilon_0 D_p kT/e^2} \tag{2}$$

   where $\Phi = \frac{e}{\sqrt{4\pi^2\varepsilon_0 D_p kT}}$, e is the elementary charge, ε_0 is the dielectric constant of air, k is the Boltzmann constant, T is absolute temperature, and $Z_{i+}/Z_{i-} = 0.875$ is the ion mobility ratio [*TSI*, 2003].

   Calculation of the mobility diameter is done using the fundamental DMA equation [*Wang and Flagan*, 1989]:

$$\frac{D_p}{nC_c(D_p)} = \frac{2eV(t)}{3\mu q_s ln\frac{r_1}{r_2}} \tag{3}$$

   where $C_c(D_p) = 1 + \frac{2\lambda}{D_p}\left[1.257 + 0.4\exp\left(\frac{-1.1D_p}{2\lambda}\right)\right]$ is the size-dependent Cunningham slip correction factor [*Seinfeld and Pandis*, 2006], $V(t)$ is the applied voltage at a given time t during the scan, μ is the viscosity of air, q_s is the sheath flow rate, and r_1, r_2 are the inner and outer radii of the DMA annular space, respectively.

5. The CCN timeseries is processed similarly to the CN timeseries, with the difference that the CCN counts in each size bin j is multiplied by $R_a^*(D_{p_j})$.

6. The processed CCN and CN timeseries are used to update $R_a^*(D_p)$; Steps 4-6 are iterated until convergence of $R_a(D_p)$ (typically within 2-3 iterations).

7. The CCN number size distribution at the instrument supersaturation, $n_s(D_p)$, is given by $n_s(D_p) = R_a(D_p)n_n(D_p)$.

The above algorithm is one of numerous approaches presented in the literature to correct for multiply-charged particles in size-resolved CCN measurements using electrical mobility classification. *Frank et al.* [2006] corrected for multiple charging by removing the fraction of particles with +2 or more charges scaled by an activation efficiency determined from an average of five spectra. *Rose et al.* [2008] assumed a constant fraction of doubly-charged particles across the entire size distribution as determined from the hump of the CCN/CN response curve and subtracted from fraction from the CCN and CN distributions. *Petters et al.* [2007] fit the CCN and CN response curves to a function that incorporates the size-dependent DMA transfer function, multiple charge fraction, and activation efficiency. By iteratively minimizing the χ^2 statistic, the activation efficiency of the particle distribution can be determined with a substantial fraction of multiply-charged particles. *King et al.* [2009] simulate the instrument response by employing a function similar to *Petters et al.* [2007], but with a binary activation efficiency (being unity if activated, or zero if unactivated) based on the size-dependent critical supersaturation computed from Köhler Theory (using measured composition and assumed organic properties). *Petters et al.* [2009] developed a matrix form of the inversion used by *Petters et al.* [2007] to calculate the activation efficiency from the measured CCN and CN size distribution without an iterative process. All the above methods do not employ the DMA in scanning voltage mode.

Particle sphericity is often assumed to determine the diameter corresponding to the centroid mobility of each size bin; this may lead to important sizing biases for non-spherical particles (e.g., black carbon, mineral dust, or crystalline inorganics). This issue can be accounted for by using a "dynamic shape factor", which accounts for the difference in hydrodynamic drag force experience by a non-spherical particle compared to a spherical particle of the same mass. Shape factors for pure salts are often known (e.g., 1.08 for NaCl, *Kämer et al.* [2000]), but its determination for ambient particles may require auxiliary measurements of aerodynamic sizing (e.g., *DeCarlo et al.* [2004]; *Kuwata and Kondo* [2009]).

3. Measurement Uncertainty

As with all particle detection methods, sufficient counting statistics are required to obtain meaningful distributions. Both the CFSTGC and the CPC accumulate counts, N, over a time period τ_{accum}. N is then divided by the volume of aerosol sample, Q_a, that flows through the optics (during τ_{accum}) to provide the concentration of CN, CCN (C_{CN}, C_{CCN}). The relative uncertainty in concentration, ε_C, is then determined from the relative counting uncertainty, ε_N, and the flow rate uncertainty, ε_{Q_a}, as

$$\varepsilon_C^2 = \left(\frac{\sigma_C}{C}\right)^2 = \varepsilon_N^2 + \varepsilon_{Q_a}^2 \tag{4}$$

where σ_C is the absolute concentration uncertainty and ε_N, ε_{Q_a} are the relative uncertainties of N and Q_a, respectively. Q_a is continuously measured in the instrument, so ε_{Q_a} can be directly determined as $\frac{\sigma_{Q_a}}{Q_a}$. The CFSTGC samples at a lower flow rate (0.018–0.25 L min^{-1}) than either of the CPCs in this work. For the CFSTGC, ε_{Q_a} almost never exceeded 4%, reported flow rate uncertainties for the TSI 3010 CPC and TSI 3022a CPC are 10% and 5%, respectively. Assuming that particles are randomly distributed in space throughout the sampled volume, Poisson statistics can be used to estimate ε_N, since the sample standard deviation equals the square root of the mean ($\varepsilon_N = \frac{\sigma_N}{N} = N^{-1/2}$). Accumulating counts over τ_{accum} seconds, yields a modified form of Equation 4,

$$\varepsilon_C^2 = \left(\frac{CQ_a}{\tau_{accum}}\right)^{-1} + \varepsilon_{Q_a}^2 \tag{5}$$

Then, the combination of applying 5 for C_{CCN} and C_{CN} yields the uncertainty for the activation efficiency, $R_a = \frac{C_{CCN}}{C_{CN}}$, as

$$\varepsilon_{R_a}^2 = \left(\frac{C_{CN}Q_{CN}}{\tau_{accum}}\right)^{-1} + \left(\frac{C_{CCN}Q_{CCN}}{\tau_{accum}}\right)^{-1} + \varepsilon_{Q_{CCN}}^2 + \varepsilon_{Q_{CN}}^2 \tag{6}$$

Table 1 provides values of $\varepsilon_{C_{CCN}}$ and $\varepsilon_{C_{CN}}$ for selected values of C_{CN} (evaluated at $R_a = 0.5$). A sample flow rate in the CFSTGC of 0.045 L min^{-1} is assumed (total flow rate of 0.5 L min^{-1}, 10:1 sheath-to-aerosol flow ratio) and a 0.3 L min^{-1} internal flow rate is assumed for the TSI 3022a CPC. Thus, for most atmospherically-relevant CN concentrations, $\varepsilon_{C_{CN}}$ is 7% or less, while $\varepsilon_{C_{CCN}}$ is less than 17% and ε_{R_a} is less than 18%.

The validity of applying Poisson statistics to approximate the concentration uncertainty was confirmed

Table 1. Calculated relative uncertainty in CN Concentration, C_{CN}, CCN Concentration, C_{CCN}, and Activated Ratio, R_a, (evaluated at R_a=0.5) for selected values of C_{CN}.

C_{CN} (cm^{-3})	$\varepsilon_{C_{CCN}}$	$\varepsilon_{C_{CN}}$	ε_{R_a}
20	0.37	0.11	0.38
100	0.17	0.067	0.18
200	0.12	0.059	0.14
1000	0.065	0.052	0.083
2000	0.054	0.051	0.074

experimentally by activation of classified $(NH_4)_2SO_4$ aerosol of 80-600 nm diameter at CFSTGC supersaturations between 0.16% and 0.39%. A comparison between predicted and observed ε_N exhibits excellent agreement (not shown).

4. Evaluation of SMCA

4.1. SMCA for laboratory aerosol

SMCA was evaluated using aerosol generated via atomization of an aqueous salt solution, followed by drying of the droplets with silica gel diffusion dryers. The dry polydisperse aerosol was introduced into a DMA, which was operated using both SMCA and "stepping mode". Figure 3 displays R_a as a function of mobility diameter, when the DMA is operated in scanning mode (closed symbols) and stepping mode (open symbols). Data is shown for aerosol composed of $(NH_4)_2SO_4$ (top panel) and NaCl (bottom panel). Noted on each curve is the temperature difference across the growth chamber used to generate supersaturation. Ordinate error bars represent the standard deviation of 3 scan repetitions (at each size); abscissa error bars are the half-width of the DMA transfer function (±5% for the 10:1 sheath-to-aerosol ratio used). Activation curves obtained using SMCA and "stepping mode" of the DMA are largely identical. There is a slight "broadening" of the activation curves at the lower ΔT (supersaturation) associated with the OPC integration time (which is enhanced at large particle sizes). This issue could be addressed by increasing the voltage scan time at low supersaturations, or accounting for the integration time in the inversion (e.g., *Russell et al.* [1995]; *Collins et al.* [2002]). The experiments for obtaining scanning mode curves in Figure 3 were performed in approximately 20 minutes.

The activation curves display a characteristic "sigmoidal" shape; the dry diameter, d_{p50}, for which 50% activation of the calibration particles act as CCN is called "dry activation diameter". Figure 3 shows the activation curves with multiple charge correction. Prior to correction, minor secondary activation peak to the left of d_{p50} was observed (Figure 4). When multiple charge correction is applied, the secondary peak vanishes, and the slope of the sigmoid steepens (Figure 4). The relative uncertainty in d_{p50} associated with neglecting multiple charges is approximately 3-4%, consistent with the results of *Rose et al.* [2008] (whom operated the DMA in "voltage-stepping" mode).

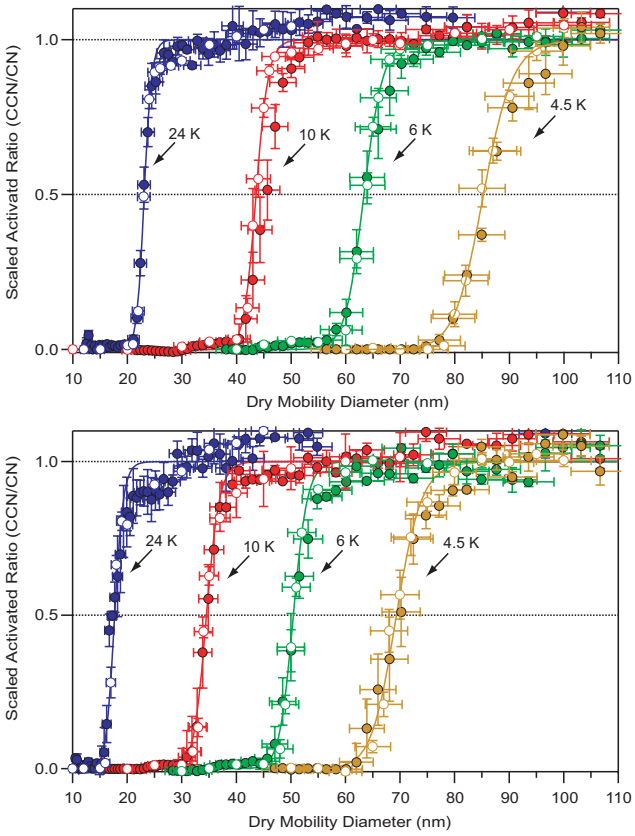

Figure 3. Example of activation curves obtained by SMCA (filled symbols) and by stepping-mode measurements (open symbols). Top panel is for activation of $(NH_4)_2SO_4$ aerosol, while bottom is for NaCl aerosol. Noted on each curve is the temperature difference across the growth chamber used to generate supersaturation. All curves were corrected for multiple charges using the algorithm described in the text. Explanation of error bars is provided in the text.

d_{p50} corresponds to the particle with critical supersaturation equal to the instrument supersaturation, and should not change if the DMA is operated in "stepping" or "scanning" mode. This is shown in Figure 5a,

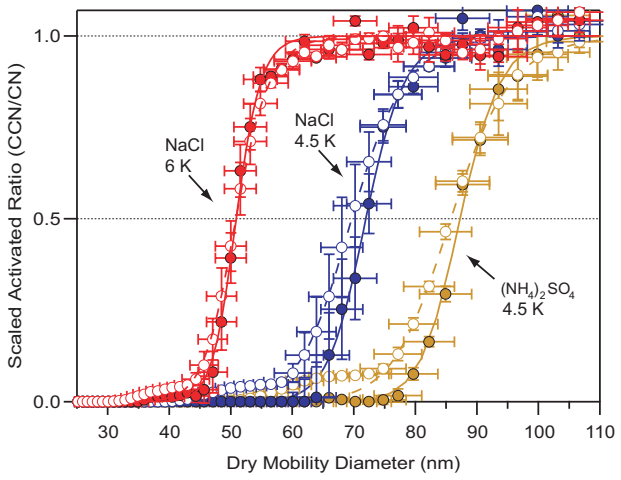

Figure 4. Activation curves obtained by SMCA. Shown are inversions without (open symbols) and with multiple-charge corrections (filled symbols). Noted on each curve are the aerosol composition and the temperature difference across the growth chamber used to generate supersaturation.

which presents d_{p50} (determined by both methods) for $(NH_4)_2SO_4$ (open symbols) and NaCl (filled symbols) aerosol. Error bars represent the half-width of the DMA transfer function (±5%). The excellent agreement in d_{p50} between both methods implies that calibration of instrument supersaturation should also be in agreement. This is shown in Figure 5b; Köhler Theory [*Seinfeld and Pandis*, 2006] is applied to compute the critical supersaturation of particles s_c from knowledge of d_{50} and chemical composition:

$$s_c = \left(\frac{4A^3}{27B}\right)^{1/2} \tag{7}$$

where $A = \frac{4M_w\sigma_w}{\rho_w RT}$, $B = \frac{\phi_s \nu_s \rho_s d_{50}^3}{\rho_w M_w}$ and M_w, σ_w, rho_w is the molar mass, surface tension and density of water, respectively. ϕ_s, ν_s, and ρ_s are the osmotic coefficient, stoichiometric van't Hoff factor, and density of the solute, respectively. A dynamic shape factor of 1.08 was applied to d_{50} to account for the non-sphericity of NaCl [*Kämer et al.*, 2000]. ϕ_s accounts for incomplete solute dissociation and was calculated for $(NH_4)_2SO_4$ and NaCl using the ion-interaction approach of *Pitzer and Mayorga* [1973] with parameters taken from *Clegg and Brimblecombe* [1988]. Instrument supersaturation calibrated by "stepping" or "scanning" modes are virtually identical; at the lower supersaturation, there is a minor (∼3%) difference in supersaturation from the

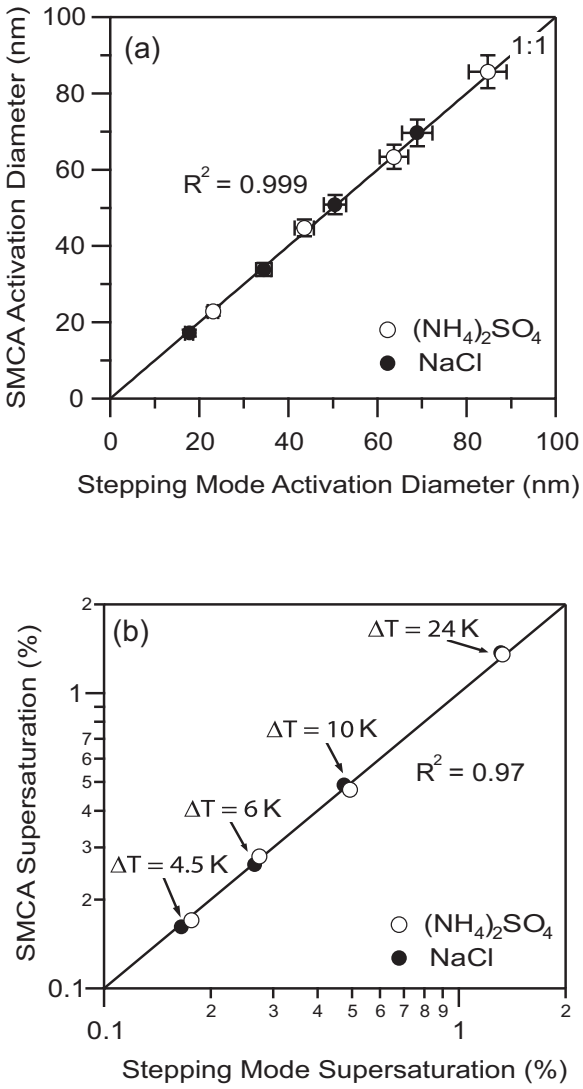

Figure 5. (a) Dry activation diameter determined by SMCA and stepping mode operation for $(NH_4)_2SO_4$ and NaCl particles. Explanation of error bars is provided in the text. (b) Instrument supersaturation calibration as determined by SMCA and stepping mode operation for $(NH_4)_2SO_4$ and NaCl particles. Results shown for different column temperature gradients.

smearing effect of the long integration time of the CF-STGC OPC.

SMCA also allows for the measurement of the size of activated CCN (droplets) exiting the flow chamber, as a function of particle dry diameter. An example is shown in Figure 6, where the (wet) size of the activated CCN detected in the OPC is plotted against dry

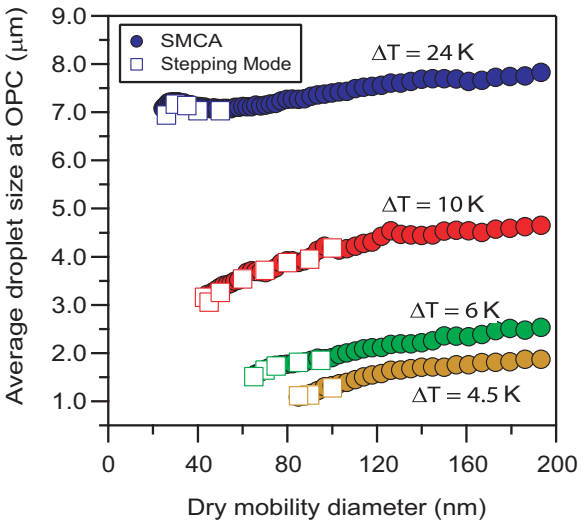

Figure 6. Size of activated $(NH_4)_2SO_4$ particles measured at the OPC of the CCN instrument, as a function of dry mobility diameter and instrument supersaturation for the data presented in Figure 3.

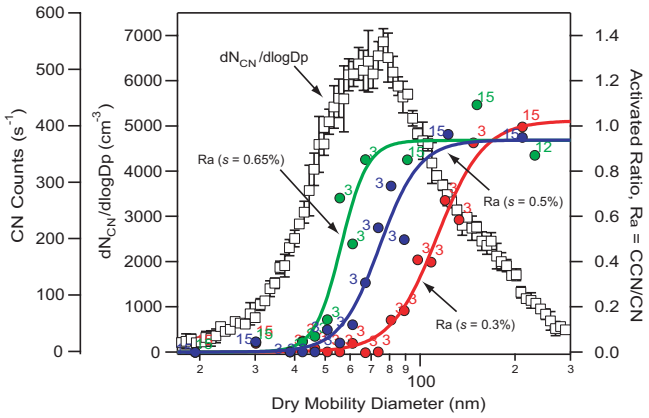

Figure 7. Example of differential activation spectra obtained by SMCA with multiple-charge correction for aerosol sampled at the AIRMAP Thompson Farm site during the NEAQS-ITCT2K4 campaign. The limited counting statistics are addressed by averaging (post-measurement) consecutive 1s bins, the number of which is noted beside each point.

mobility diameter, determined from SMCA (filled symbols) and "stepping mode" (open symbols) operation of the DMA. Data is shown for a number of supersaturation levels in the CFSTGC. As expected, the droplet size at constant supersaturation increases with aerosol dry diameter [*Lance et al.*, 2006]; exposing particles of constant dry diameter to higher supersaturation also increases the droplet diameter at detection [*Lance et al.*, 2006]. Diameters using both modes of DMA operation are in excellent agreement.

4.2. SMCA for ambient aerosol

SMCA was used for ambient aerosol measurements obtained at the University of New Hampshire (UNH) AIRMAP Observing Station (http://airmap.unh.edu) at Thompson Farm. The site is located in Durham, NH, approximately two miles south of the University of New Hampshire (43.11N, 70.95W, elevation 75ft). The aerosol at this location is an internal mixture of organic and inorganic material and is ideal for evaluating SMCA. A detailed description of the station and dataset can be found in *Medina et al.* [2007]; data shown here were collected on August 8^{th}, 2004, during the NEAQS-ITCT2K4 campaign (July-August 2004).

Figure 7 presents exemplary aerosol size distributions and activation efficiency curves sampled at three different supersaturations. As expected, the CCN distribution increasingly converges towards the total aerosol number size distribution as the instrument supersaturation increases. If particle composition is size-invariant, the CCN distribution would be zero for all sizes less than a single characteristic value (i.e., where the particle critical supersaturation equals the instrument supersaturation), and the sigmoidal activation curve would appear as a step function. This is not the case however in Figure 7, as chemical heterogeneity (size-dependant composition and mixing state) broadens the transition towards activation.

We test SMCA by assessing "closure" with another CCN instrument. This is done by comparing total CCN concentrations obtained by integration of the differential size spectra (like those in Figure 7) with measurements obtained independently with another CCN instrument measuring the total aerosol distribution. The CCN concentrations from the integrated SMCA distributions agree with CCN measurements obtained with the other CFSTGC to within measurement variability (Figure 8).

5. Summary-Conclusions

We present Scanning Mobility CCN Analysis (SMCA), a novel method for obtaining fast measurements of size-resolved CCN activity and growth kinetics, by coupling a CPC and a CCN counter with the monodisperse outlet stream of a scanning DMA. By applying the same

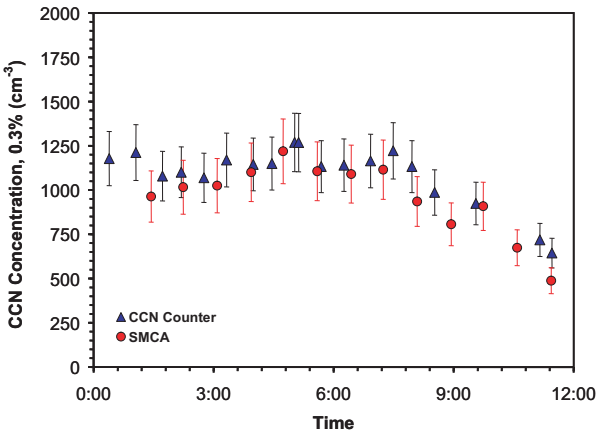

Figure 8. CCN concentrations at 0.3% supersaturation for in-situ aerosol sampled during the NEAQS-ITCT2K4 campaign. Shown are results obtained from direct measurements of CCN (triangles) and integrated SMCA spectra (circles).

inversion algorithm as is currently used for obtaining size distributions, CCN activity and droplet growth kinetics are obtained as a function of mobility size over the timescale of a SMPS scan. The performance of the new method is evaluated for activation of laboratory-generated aerosol composed of $(NH_4)_2SO_4$, NaCl and for ambient aerosol measured at the AIRMAP Thompson Farm site during the ITCT2K4 field campaign. Overall, SMCA performs remarkably well, as essentially identical CCN properties are seen measured with "scanning" and "stepping" modes of the DMA.

SMCA has been successfully used in studies focused on size-resolved CCN measurements [e.g., *Padró et al.*, 2007; *Asa-Awuku et al.*, 2008, 2010, 2009; *Engelhart et al.*, 2008; *Moore et al.*, 2008; *Padró et al.*, 2010]. The fast time response and ease of setting up SMCA are attractive features, especially if measurements are to be carried out in polluted environments and the laboratory (where counting statistics are most favorable for rapid measurements). SMCA can also be used to study the size-resolved CCN activity in clean environments, at the expense of some temporal (or size) resolution. Finally, SMCA can be applied to commercial SMPS and CFSTGC instruments with the manufacturer-provided control software coupled with a simple post-processing routines (available for download from http://nenes.eas.gatech.edu) to align the instrument response curves, correct for multiple charges, and correct for the non-sphericity of the aerosol.

Acknowledgments. We acknowledge the support of a National Science Foundation CAREER award and the National Oceanic and Atmospheric Administration under grant NA04OAR4310088. RHM acknowledges support from a DOE Graduate Research Environmental Fellowship and a Georgia Tech Presidential Fellowship. JM acknowledges support from a NASA Earth System Science Fellowship. We thank A.Asa-Awuku, K.Bougiatioti, G.Engelhart, P.Kumar, T.Lathem, L.Padró and T.Raymond for their feedback on the SMCA inversion software. We also thank S.Lance, three anonymous reviewers and the editor (S.Hering) for feedback that substantially improved the manuscript.

References

Asa-Awuku, A., A. Nenes, A. Sullivan, C. Hennigan, and R. Weber, Investigation of molar volume and surfactant characteristics of water-soluble organic compounds in biomass burning aerosol, *Atmos. Chem. Phys.*, *8*, 799–812, 2008.

Asa-Awuku, A., G. Engelhart, B. Lee, S. Pandis, and A. Nenes, Relating CCN activity, volatility, and droplet growth kinetics of β-caryophyllene secondary organic aerosol, *Atmos. Chem. Phys.*, *9*, 795–812, 2009.

Asa-Awuku, A., A. Nenes, S. Gao, R. Flagan, and J. Seinfeld, Water-soluble SOA from alkene ozonolysis: composition and droplet activation kinetics inferences from analysis of CCN activity, *Atmos. Chem. Phys.*, *10*, 1585–1597, 2010.

Bougiatioti, A., C. Fountoukis, N. Kalivitis, S. Pandis, A. Nenes, and N. Mihalopoulos, Cloud condensation nuclei measurements in the marine boundary layer of the Eastern Mediterranean: CCN closure and droplet growth kinetics, *Atmos. Chem. Phys.*, *9*, 7053–7066, 2009.

Broekhuizen, K., R. Chang, W. Leaitch, S. Li, and J. P. D. Abbatt, Closure between measured and modeled cloud condensation nuclei (CCN) using size-resolved aerosol compositions in downtown Toronto, *Atmos. Chem. Phys.*, *6*, 2513–2524, 2006.

Carrico, C., M. Petters, S. Kreidenweis, J. C. Jr., G. Engling, and W. Malm, Aerosol hygroscopicity and cloud droplet activation of extracts of filters from biomass burning experiments, *J. Geophys. Res.*, *113*, D08,206, 2008.

Clegg, S. L., and P. Brimblecombe, Equilibrium partial pressures of strong acids over concentrated saline solutions - I. HNO_3, *Atmos. Environ.*, *22*, 91–100, 1988.

Collins, D., R. Flagan, and J. Seinfeld, Improved inversion of scanning DMA data, *Aerosol Sci. Technol.*, *36*, 1–9, 2002.

Crump, J., and J. Seinfeld, A new algorithm for inversion of aerosol size distribution data, *Aerosol Sci. Technol.*, *1*, 1534, 1982.

Cubison, M., B. Ervens, G. Feingold, K. Docherty, I. Ulbrich, L. Shields, K. Prather, S. Hering, and J. Jimenez, The influence of chemical composition and mixing state of Los Angeles urban aerosol on CCN number and cloud properties, *Atmos. Chem. Phys.*, *8*, 5649–5667, 2008.

DeCarlo, P. F., J. G. Slowik, D. R. Worsnop, P. Davidovits, and J. L. Jimenez, Particle morphology and density characterization by combining mobility and aerodynamic diameter measurements. Part 1: Theory, *Aerosol Sci. Technol.*, *38*, 11851205, 2004.

Dusek, U., G. Frank, J. Curtius, F. Drewnick, J. Schneider, A. Küten, D. Rose, M. Andreae, S. Borrmann, and U. Pöschl, Enhanced organic mass fraction and decreased hygoscopicity of cloud condensation nuclei (CCN) during new particle formation events, *Geophys. Res. Lett.*, *37*, L03,804, 2010.

Engelhart, G., A. Asa-Awuku, A. Nenes, and S. N. Pandis, CCN activity and droplet growth kinetics of fresh and aged monoterpene secondary organic aerosol, *Atmos. Chem. Phys.*, *8*, 3937–3949, 2008.

Frank, G., U. Dusek, and M. Andreae, Technical note: A method for measuring size-resolved CCN in the atmosphere, *Atmos. Chem. Phys. Discuss.*, *6*, 4879–4895, 2006.

Gunn, R., The statistical electrification of aerosols by ionic diffusion, *J.Coll.Sci.*, *10*, 107–119, 1955.

Gunn, R., and R. Woessner, Measurements of the systematic electrification of aerosols, *J.Coll.Sci.*, *11*, 254–259, 1956.

Gunthe, S., S. King, D. Rose, Q. Chen, P. Roldin, D. Farmer, J. Jimenez, P. Artaxo, M. Andreae, S. Martin, and U. Pöschl, Cloud condensation nuclei in pristine tropical rainforest air of amazonia: size-resolved measurements and modeling of atmospheric aerosol composition and CCN activity, *Atmos. Chem. Phys.*, *9*, 7551–7575, 2009.

Hagen, D., and D. Alofs, Linear inversion method to obtain aerosol size distributions from measurements with a differential mobility analyzer, *Aerosol Sci. Technol.*, *2*, 465–475, 1983.

Intergovernmental Panel on Climate Change (IPCC), *Climate Change 2007: The Physical Science Basis: Summary for Policymakers*, 2007.

International Aerosol Precipitation Science Assessment Group (IAPSAG), *Air Pollution Impact on Precipitation: A Scientific Review*, 2007.

Jurányi, Z., M. Gysel, E. Weingartner, P. DeCarlo, L. Kammermann, and U. Baltensperger, Measured and modelled cloud condensation nuclei concentration at the high alpine site Jungfaujoch, *Atmos. Chem. Phys. Discuss.*, *10*, 8859–8897, 2010.

Kämer, L., U. Pöschl, and R. Niessner, Microstructural rearrangement of sodium chloride condensation aerosol particles on interaction with water vapor, *J. Aerosol Sci.*, *31*, 673–685, 2000.

King, S., T. Rosenoern, J. Shilling, Q. Chen, and S. Martin, Increased cloud activation potential of secondary organic aerosol for atmospheric mass loadings, *Atmos. Chem. Phys.*, *9*, 2959–2972, 2009.

Kuwata, M., and Y. Kondo, Measurements of particle masses of inorganic salt particles for calibration of cloud condensation nuclei counters, *Atmos. Chem. Phys.*, *9*, 5921–5932, 2009.

Kuwata, M., Y. Kondo, Y. Miyazaki, Y. Komazaki, J. H. Kim, S. S. Yum, H. Tanimoto, and H. Matsueda, Cloud condensation nuclei activity at Jeju Island, Korea in spring 2005, *Atmos. Chem. Phys.*, *8*, 2933–2948, 2008.

Lance, S., Quantifying compositional impacts of ambient aerosol on cloud droplet formation, Ph.D. thesis, Georgia Institute of Technology, Atlanta, GA, 2007.

Lance, S., J. Medina, J. Smith, and A. Nenes, Mapping the operation of the DMT continuous flow CCN counter, *Aerosol Sci. Technol.*, *40*, 242–254, 2006.

Lance, S., A. Nenes, C. Mazzoleni, M. Dubey, H. Gates, V. Varutbangkul, T. A. Rissman, S. M. Murphy, A. Sorooshian, F. Brechtel, R. Flagan, J. Seinfeld, G. Feingold, and H. Jonsson, CCN activity, closure and droplet growth kinetics of Houston aerosol during the Gulf of Mexico Atmospheric Composition and Climate Study (GoMACCS), *J. Geophys. Res.*, *114(D00F15)*, 2009.

Medina, J., A. Nenes, R. Sotiropoulou, L. Cottrell, L. Ziemba, P. Beckman, and R. Griffin, Cloud condensation nuclei (CCN) closure during the ICARTT 2004 campaign: effects of size-resolved composition, *J. Geophys. Res.*, *112*, doi:110.1029/2006JD007,588, 2007.

Moore, R., and A. Nenes, Scanning flow CCN analysis - a method for fast measurements of CCN spectra, *Aerosol Sci. Technol.*, *43*, 1192–1207, 2009.

Moore, R. H., E. D. Ingall, A. Sorooshian, and A. Nenes, Molar mass, surface tension, and droplet growth kinetics of marine organics from measurements of CCN activity, *Geophys. Res. Lett.*, *35*, 2008.

Padró, L., Towards an understanding of the cloud formation potential of carbonaceous aerosol: Laboratory and field studies, Ph.D. thesis, Georgia Institute of Technology, Atlanta, GA, 2009.

Padró, L., A. Asa-Awuku, R. Morrison, and A. Nenes, Inferring thermodynamic properties from CCN activation experiments: Single-component and binary aerosols, *Atmos. Chem. Phys.*, *7*, 5263–5274, 2007.

Padró, L., D. Tkacik, T. Lathem, C. Hennigan, A. Sullivan, R. Weber, L. Huey, and A. Nenes, Investigation of CCN relevant properties and droplet growth kinetics of water-soluble aerosol fraction in Mexico City, *J. Geophys. Res.*, *115(D09204)*, 2010.

Petters, M., and S. Kreidenweis, A single parameter representation of hygroscopic growth and CCN activity, *Atmos. Chem. Phys.*, *7*, 1961–1971, 2007.

Petters, M., A. Prenni, S. Kreidenweis, and P. DeMott, On measuring the critical diameter of cloud condensation nuclei using mobility selected aerosol, *Aerosol Sci. Technol.*, *41*, 907–913, 2007.

Petters, M., C. Carrico, S. Kreidenweis, A. Prenni, P. DeMott, J. C. Jr., and H. Moosmuller, Cloud condensation nucleation activity of biomass burning aerosol, *J. Geophys. Res.*, *114*, D22,205, 2009.

Pitzer, K., and G. Mayorga, Thermodynamics of electrolytes. II. activity and osmotic coefficients for strong electrolytes with one or both ions univalent, *J. Phys. Chem.*, *77*, 2300–2308, 1973.

Roberts, G., and A. Nenes, A continuous-flow streamwise thermal-gradient CCN chamber for atmospheric measurements, *Aerosol Sci. Technol.*, *39*, 206–221, 2005.

Rose, D., S. Gunthe, E. Mikhailov, G. Frank, U. Dusek, M. Andreae, and U. Pöschl, Calibration and measurement uncertainties of a continuous-flow cloud condensation nuclei counter (DMT-CCNC): CCN activation of ammonium sulfate and sodium chloride aerosol particles in theory and experiment, *Atmos. Chem. Phys.*, *8*, 1153–1179, 2008.

Rose, D., A. Nowak, P. Achtert, A. Wiedensohler, M. Hu, M. Shao, Y. Zhang, M. Andreae, and U. Pöschl, Cloud condensation nuclei in polluted air and biomass burning smoke near the mega-city Guangzhou, China - Part 1: Size-resolved measurements and implications for the modeling of aerosol particle hygroscopicity and CCN activity, *Atmos. Chem. Phys.*, *10*, 3365–3383, 2010.

Ruehl, C., P. Chuang, and A. Nenes, Distinct CCN activation kinetics above the marine boundary layer along the California coast, *Geophys. Res. Lett.*, *36*, 2009.

Ruehl, C. P., C.R., and A. Nenes, How quickly do cloud droplets form on atmospheric particles?, *Atmos. Chem. Phys.*, *8*, 1043–1055, 2008.

Russell, L., R. Flagan, and J. Seinfeld, Asymmetric instrument response resulting from mixing effects in accelerated DMA-CPC measurements, *Aerosol Sci. Technol.*, *23*, 491509, 1995.

Seinfeld, J., and S. Pandis, *Atmospheric chemistry and physics: from air pollution to climate change*, 2nd ed., John Wiley, New York, 2006.

Shantz, N. C., W. R. Leaitch, L. Phinney, M. Mozurkewich, and D. Toom-Sauntry, The effect of organic compounds on the growth rate of cloud droplets in marine and forest settings, *Atmos. Chem. Phys.*, *8*, 5869– 5887, 2009.

Shinozuka, Y., A. D. Clarke, P. F. DeCarlo, J. L. Jimenez, E. J. Dunlea, G. C. Roberts, J. M. Tomlinson, D. R. Collins, S. G. Howell, V. N. Kapustin, C. S. McNaughton, and J. Zhou, Aerosol optical properties relevant to regional remote sensing of CCN activity and links to their organic mass fraction: airborne observations over Central Mexico and the US West Coast during MILAGRO/INTEX-B, *Atmos. Chem. Phys.*, *9*, 67276742, 2009.

Sorooshian, A., S. Murphy, S. Hersey, H. Gates, L. Padró, A. Nenes, R. F. F. Brechtel, H. Jonsson, and J. Seinfeld, Comprehensive airborne characterization of aerosol from a major bovine source, *Atmos. Chem. Phys.*, *8*, 5489–5520, 2008.

TSI, 3936 Scanning Mobility Particle Sizer manual, *Instrument manual*, 2003.

Vestin, A., J. Rissler, E. Swietlicki, G. Frank, and M. Andreae, Cloud-nucleating properties of the amazonian biomass burning aerosol: Cloud condensation nuclei measurements and modeling, *J. Geophys. Res.*, *112*, D14,201, 2007.

Wang, J., Y. Lee, P. Daum, J. Jayne, and M. Alexander, Effects of aerosol organics on cloud condensation nucleus (CCN) concentration and first indirect aerosol effect, *Atmos. Chem. Phys.*, *8*, 6325–6339, 2008.

Wang, S., and R. Flagan, Scanning electrical mobility spectrometer, *J. Aerosol Sci.*, *20*, 14851488, 1989.

Wex, H., T. Hennig, I. Salma, R. Ocskay, A. Kiselev, S. Henning, A. Massling, A. Wiedensohler, and F. Stratmann, Hygroscopic growth and measured and modeled critical supersaturations of an atmospheric HULIS sample, *Geophys. Res. Lett.*, *34*, doi: 10.102/2006GL028,260, 2007.

Wiedensohler, A., Technical note: An approximation of the bipolar charge distribution for particles in the submicron range, *J. Aerosol Sci.*, *19*, 387–389, 1988.

A. Nenes, Schools of Earth & Atmopsheric Sciences and Chemical & Biomolecular Engineering, Georgia Institute of Technology, Atlanta, GA 30332 (e-mail: athanasios.nenes@gatech.edu)

R. Moore, School of Chemical & Biomolecular Engineering, Georgia Institute of Technology, Atlanta, GA 30332 (e-mail: richard.moore@chbe.gatech.edu)

J. Medina, School of Chemical & Biomolecular Engineering, Georgia Institute of Technology, Atlanta, GA 30332 (e-mail: jeessy.medina@chbe.gatech.edu)

Received N/A; revised N/A; accepted N/A.